High-Performance Graphene-on-Silicon Nitride All-Optical Switch Based on a Mach–Zehnder Interferometer

Ciyuan Qiu, *Member, IEEE, Member, OSA*, Can Zhang, Huiying Zeng, and Tao Guo

***Abstract*—We propose and experimentally demonstrate a high-performance graphene-on-silicon nitride (Si_3N_4) all-optical switch based on a Mach–Zehnder interferometer (MZI). In our device, the graphene overlaying on a Si_3N_4 waveguide absorbs part of the pump light power and generates heat. Then, the Si_3N_4 waveguide underneath can be heated and its refractive index can be changed due to the thermo-optic effect. In this way, the phase of the probe light in the Si_3N_4 arm with graphene on top is tuned and all optical switching can then be implemented. In the experimental demonstration, an all-optical switch with a chip size of $\sim$0.36 mm^2 is realized with an extinction ratio of 11 dB. The tuning efficiency is measured to be 0.00917 π/mW, which is insensitive to the wavelength of the pump light. All-optical switching is also demonstrated, while the rise and fall time constants are measured to be 571 ns and 1.29 μs, respectively. These results show that our proposed configuration provides a functional integrated component for the development of efficient all-optical control devices with a fast switching speed on the insulator platform. Moreover, by using integrated MZI structure, our design could potentially achieve a broad bandwidth.**

***Index Terms*—All-optical switch, graphene, Mach–Zehnder interferometer, silicon nitride.**

I. Introduction

ALL-OPTICAL switches are key components in all optical signal processing which avoids Optical-Electrical-Optical (OEO) conversion and thus has the potential to achieve a power efficient photonic system [1]. Recently, fiber-based all-optical switches have been explored for achieving efficient all-optical light control [2], [3]. Moreover, to implement a large-scale photonic system, on-chip integration is highly desired. To date, a large number of integrated all-optical switches have been built on semiconductor platforms, including silicon and InP [4]–[6], etc. However, due to their finite bandgaps, two-photon absorption (TPA) effect and free-carrier absorption (FCA) effect exist in these semiconductor materials at telecommunication wavelength, which results in large propagation losses and high power consumptions [7].

To eliminate the TPA and FCA losses for integrated all-optical switches, silicon nitride (Si_3N_4) offers new opportunities since it is insulator material with a large bandgap [8], [9]. In addition, Si_3N_4 possesses many other appealing properties, such as CMOS process compatibility, high fabrication tolerance resulting from the low refractive index contrast, and low propagation loss compared with silicon [10], [11]. Therefore, Si_3N_4 platform is possible to achieve simple fabrication processes and low nonlinear losses. However, as an insulator material, Si_3N_4 material has a weak thermo-optic effect, i.e., the thermal conductivity (30 W·m^{-1} K^{-1})[12] and thermo-optic coefficient (2.5×10^{-5} K^{-1}) [13] of Si_3N_4 are much weaker than those of silicon (130 W·m^{-1}·K^{-1} and 1.8×10^{-4} K^{-1}) [14]. Then, for the all-optical switching based on the thermo-optic tuning, the weak thermo-optic effect of Si_3N_4 would increase the power consumption and lead to a low tuning efficiency. Thus, to achieve efficient all-optical switching based on Si_3N_4 and the thermo-optic effect, a novel mechanism is highly desired.

Graphene, a two-dimensional (2D) carbon atoms material, has become a promising material in photonic applications due to its remarkable electrical and optical properties, including its linear absorption in a broad spectral range and the large nonlinearity [15], [16]. Meanwhile, with a low optical absorption rate, graphene can directly interact with waveguides, which can enhance device performances and simplify fabrication processes [17], [18]. Also, by the advantage of an extremely high thermal conductivity, graphene could overcome the shortcoming of the weak thermo-optic effect in Si_3N_4 waveguide [19]. Recently, several optical devices based on graphene-on-Si_3N_4 platform have been demonstrated [20]–[22]. Besides, We have reported a graphene-on-Si_3N_4 all-optical switch based on a micro-ring resonator (MRR) structure [23]. However, the graphene-on-Si_3N_4 MRR all-optical switch exhibits a relatively low tuning efficiency and a narrow bandwidth, which would limit it applications in all-optical signal processing.

In this paper, to enhance the tuning efficiency and obtain a broadband operation, we proposed and demonstrated a high-performance graphene-on-Si_3N_4 all-optical switch based on a Mach-Zehnder interferometer (MZI). The experimental demonstration of the MZI all-optical switch has been realized with a chip size of $\sim$0.36 mm^2 and an extinction ratio of 11 dB.

Manuscript received September 8, 2020; revised December 4, 2020; accepted December 12, 2020. Date of publication December 17, 2020; date of current version April 2, 2021. This work was supported in part by the National Key R&D Program of China under Grant 2019YFB2205204, and in part by the National Natural Science Foundation of China under Grant 61875120. *(Corresponding author: Ciyuan Qiu.)*

The authors are with the State Key Laboratory of Advanced Optical Communication Systems and Networks, Department of Electronic Engineering, Shanghai Jiao Tong University, Shanghai 200240, China (e-mail: qiuciyuan@sjtu.edu.cn; zhangcan24@sjtu.edu.cn; zenghy@sjtu.edu.cn; guotao-30@sjtu.edu.cn).

Color versions of one or more of the figures in this article are available at https://doi.org/10.1109/JLT.2020.3045472.

Digital Object Identifier 10.1109/JLT.2020.3045472

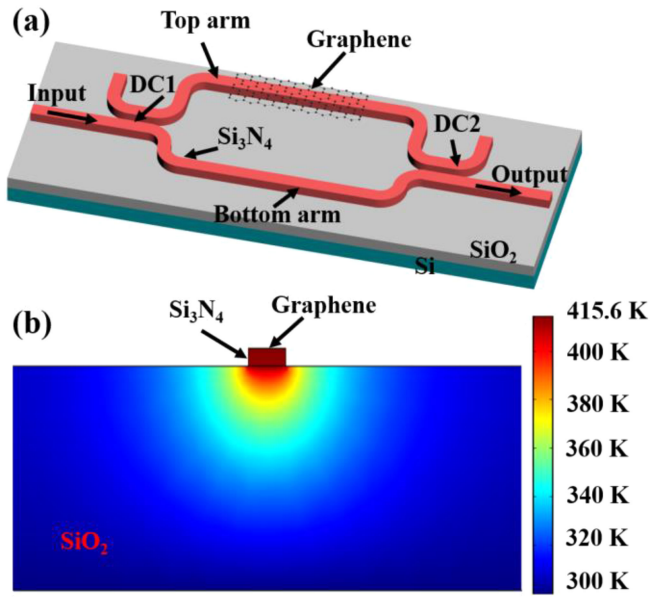

Fig. 1. (a) 3D schematic diagram of the proposed MZI all-optical switch. (b) 2D temperature distribution of the graphene-on-Si_3N_4 structure in the finite element method (FEM) simulation.

Additionally, a tuning efficiency of 0.00917 π/mW is obtained, which is ~3.6 times as high as that of our previous reported graphene-on-Si_3N_4 MRR structure [23]. Furthermore, the rise and fall time constants of the switch are measured to be 571 ns and 1.29 μs, respectively. To demonstrate the experimental results conveniently, a free spectral range (FSR) of ~8.4 nm is chosen in our experiment. Note that, the FSR is inversely proportional to the length difference between the two arms of the MZI [24], so the FSR of our device can be enlarged if the length difference decreases. Therefore, our MZI integrated switch could potentially achieve an ultra-broad bandwidth by decreasing the length difference between the two arms of the integrated MZI structure. Furthermore, the power coupling ratio of the directional couplers (DCs) of the MZI structure is also insensitive to the wavelength of the injected light. Such merits ensure the broadband operation for both pump light and probe light in the all-optical switching process. Note that, these stand in contrast to the MRR structure, in which the all-optical switching can be implemented only if both the pump light wavelength and probe light wavelength are set at the resonance wavelengths. Thus, our switch has a enhanced tuning efficiency and a broadband operation, which would make it useful in all optical switching [3], all optical logic computing [25], [26], photonic phase shifter [2], [27] as well as other on-chip all optical signal processing applications [28].

II. Device Structure and Principle

Fig. 1(a) shows the three-dimensional (3D) schematic diagram of the proposed MZI all-optical switch based on a graphene-on-Si_3N_4 hybrid structure. The proposed device consists of two different directional couplers (DC1 and DC2), two waveguide arms with different optical path lengths. Si_3N_4 waveguides with a height of 400 nm and a width of 1.2 μm are adopted to construct this device. The gap between the two waveguides of both DCs is set to 200 nm. As shown in Fig. 1(a), the input light is launched into the two arms of the MZI by DC1 and collected at the output end by DC2. Part of the top waveguide arm is covered by graphene with a length of 288 μm. Based on the numerical calculations, the propagation loss induced by graphene is estimated to be ~4.6 dB which means ~66% of the pump power in the top arm is absorbed by the graphene layer. To compensate the graphene induced propagation loss, it is required to split more optical power to the top arm. Then, the power splitting ratio of DC1 is design to be 79:21, which is realized by setting the length of DC1 to 20.7 μm. With the graphene absorption in the top waveguide arm, the optical powers at the two inputs of DC2 are then close to each other. To obtain a high-extinction ratio, the length of DC2 is thus designed to be 16.1 μm for achieving the power splitting ratio of 50:50, which is similar with that of the conventional MZI devices. To demonstrate the experimental results conveniently, the length difference between the top arm (longer) and the bottom arm is set to be 116 μm, leading to an FSR of ~8.4 nm.

The principle of our proposed device is based on the thermo-optic effect induced by the graphene. When we inject the pump light along with the probe light (signal light) into the device, the graphene overlaying on Si_3N_4 waveguide absorbs the pump light to generate heat due to the thermo-optic effect. Then, the Si_3N_4 waveguide underneath can be heated and its refractive index can be tuned. Thus, the phase shift of the probe light can be changed. In this case, optical switching is achieved by if a π-phase shift for the probe light is obtained.

To analyze the switching power and tuning efficiency of our switch, we first investigate the relationship between the injected pump power and the temperature change (ΔT) of the Si_3N_4 waveguide. The value of ΔT is estimated by using a 2D graphene-on-Si_3N_4 structure in the FEM simulation, which is illustrated in Fig. 1(b). In the simulation, the thermal conductivities of the silica, the silicon nitride, and the graphene are set to be 1.38, 29, and 2000 $W{\cdot}m^{-1}\ K^{-1}$, respectively [20], [23], [29]. Due to its high thermal conductivity, the graphene is treated as an excellent heat source. For the sake of simplicity, the longitudinal temperature distribution of the Si_3N_4 waveguide could be ignored and we just analyze the transversal temperature distribution by using the 2D graphene-on-Si_3N_4 structure [2]. Then, we assume that the heat generated by graphene is uniform on the surface of the Si_3N_4 waveguide and the heat density in the graphene layer is Q. Note that, the value of Q is related to the injected pump power P with a relationship given by:

$$Q = \frac{P \cdot K_1 \cdot \alpha}{w \cdot h \cdot l}, \tag{1}$$

where K_1 is the power splitting ratio of the top arm of DC1, α is the input pump power ratio absorbed by the graphene. According to the above-mentioned design, the K_1 value and α value are 0.79 and 0.66, respectively. And the width w, the thickness h, the length l of graphene coating on the Si_3N_4 waveguide are set to 1.2 μm, 0.5 nm, 288 μm, respectively. For a pump power P of 90 mW, the corresponding Q value is 2.69×10^{17} W/m^3. The simulated temperature change (ΔT) in the Si_3N_4 waveguide is

$\sim$115 K. Besides, the temperature change increases linearly with the pump power. For our thermo-optic devices, the refractive index change Δn caused by the temperature change is also determined by the thermo-optic coefficient ($\partial n/\partial T$) of the Si_3N_4 material, which can be represented as:

$$\Delta n = \frac{\partial n}{\partial T}\Delta T, \tag{2}$$

where the thermo-optic coefficient ($\partial n/\partial T$) of the Si_3N_4 material is $\sim 2.5 \times 10^{-5}$ K^{-1} at the wavelength around 1550 nm [13]. In this case, the phase change $\Delta\phi$ of the probe light can be evaluated by the following equation:

$$\Delta\phi = \frac{2\pi}{\lambda}\Delta n l. \tag{3}$$

where λ is the wavelength of the probe light, Δn is the refractive index change of the Si_3N_4 waveguide, l is the length of graphene coating on the Si_3N_4 waveguide. According to our design, the length of graphene coating on Si_3N_4 waveguide is 288 μm. Therefore, with a switching power of 90 mW, the probe light has a phase change of π and optical switching could be implemented. Then, the theoretical tuning efficiency of our proposed all-optical switch is 0.012 π/mW accordingly. Note that, the light absorption and then the heat generation in the Si_3N_4 waveguide is low since Si_3N_4 is an insulator material with a large bandgap. Thus, in our device, such a high tuning efficiency is due to the graphene absorption, which can efficiently generate heat and then heat the Si_3N_4 waveguide underneath.

III. Device Fabrication and Experimental Setup

A. Device Fabrication

The device was implemented on a 400-nm-thick Si_3N_4 wafer with 5-μm-thick buried oxide. The all-optical switch was firstly defined utilizing the processes of standard E-beam lithography (EBL) and inductively coupled plasma (ICP) etching. Then the 600-nm-thick silica was deposited on the surface of the device by chemical vapor deposition (CVD) process. Note that, the graphene-coating area of the top arm waveguide was not covered by silica, which was implemented by EBL and lift-off processes. In addition, we transferred the single-layer graphene onto the top arm waveguide, which was then patterned by EBL and oxygen plasma etching processes. Here, in the graphene transfer process, the graphene layer was grown on copper foil by conventional chemical vapor deposition (CVD) method. And, graphene was transferred onto the Si_3N_4/SiO_2 substrate by using a Poly(methyl methacrylate) (PMMA) assisted wet-transfer method. In this method, a PMMA layer was firstly spin-coated on graphene on the copper foil. Then, $HCl/H_2O_2/H_2O$ solution was used to etch away the copper foil. When the copper foil was completely etched, the PMMA/graphene film was moved to deionized (DI) water to rinse the etchant residue. After that, the PMMA/graphene film was scooped by the Si_3N_4/SiO_2 substrate, and then the PMMA was removed by acetone solution. Fig. 2(a) presents the microscope image of the fabricated device, in which only part of the top arm waveguide was covered by graphene. The SEM images of the graphene coating on the top arm waveguide

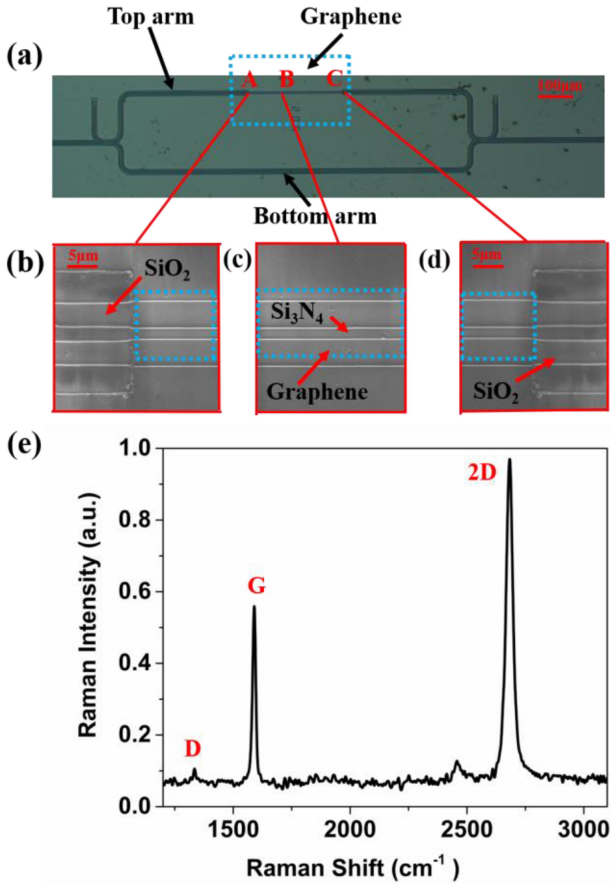

Fig. 2. (a) Microscope image of the fabricated graphene-on-Si_3N_4 all-optical switch. (b–d) Scanning electron microscopy (SEM) pictures of the graphene-coating Si_3N_4 waveguide. Note that, the area enclosed by the blue dotted line is covered by graphene. (e) Raman spectrum of the graphene overlaying on Si_3N_4 waveguide.

are provided in Fig. 2(b)$\sim$(d). The measured normalized Raman spectrum is shown in Fig. 2(e), where D peak, G peak and 2D peak lie at 1336 cm^{-1}, 1588 cm^{-1} and 2685 cm^{-1}, respectively. The 2D/G intensity ratio is measured to be $\sim$1.76, which implies the high quality of the transferred graphene overlaying on the Si_3N_4 waveguide [30], [31].

B. Experimental Setup

The experimental setup of the fabricated all-optical switch is provided in Fig. 3. Here we perform two proof-of-concept experiments, i.e., a continuous-wave (CW) tuning experiment and a dynamic switching experiment. The pump light is generated by a tunable CW laser source (TLS 150D) which is then either amplified by an Erbium-doped fiber amplifier (EDFA) for the CW tuning experiment or modulated by a commercial intensity modulator before the EDFA for the dynamic switching experiment. The wavelength of the pump light beam is set to 1550 nm, which matches the central operation wavelength of EDFA. Another broadband tunable CW laser source (Keysight 81960A) is used as the source to generate the probe light. The probe and pump light beams are adjusted to be TE polarized by polarization controllers (PCs). Then we use a 50/50 optical

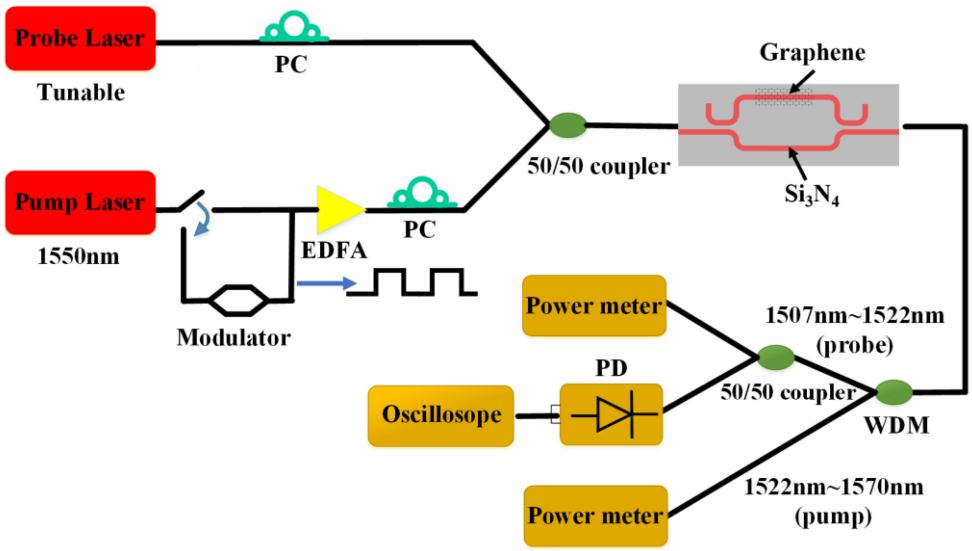

Fig. 3. Experimental setup used to characterize the performance of the fabricated all-optical switch.

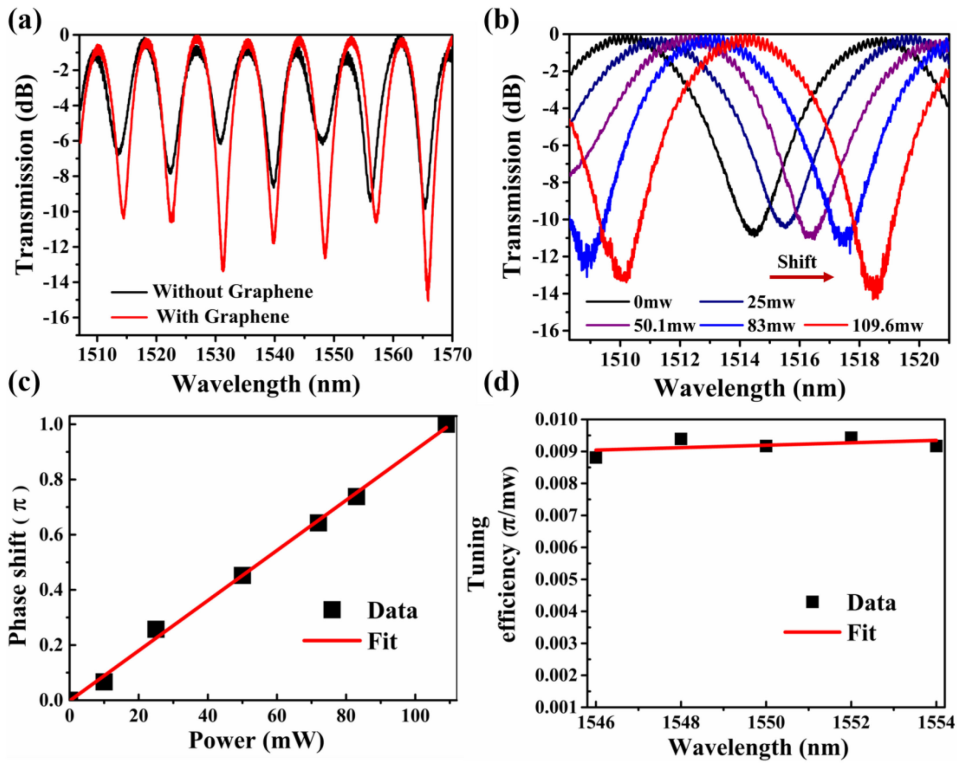

Fig. 4. (a) Normalized probe transmission spectra of the all-optical switch with and without the transferred graphene. The pump light is not applied. (b) Normalized probe transmission spectra measured at different coupled pump powers. The wavelength of the pump light is set to 1550 nm. (c) Phase shift with respect to the coupled injected pump power. (d) Tuning efficiencies at different pump light wavelengths. Here, the power of the probe light is 40 μW in the experiment.

coupler to combine the two light beams and inject them into the MZI chip through a tapered lensed fiber. After the on-chip transmission, the output light of the device is coupled out and subsequently separated into the pump light and the probe light by a wavelength division demultiplexer (WDM). Note that, after the demultiplexing, the wavelength ranges of the output probe and pump light are 1507∼1522 nm and 1522∼1570 nm, respectively. Finally, the probe light is characterized by a power meter, a photodetector and an oscilloscope.

IV. Results and Discussion

A. Tuning Efficiency

The normalized transmission spectra of the device before (black) and after (blue) transferring graphene were firstly measured as shown in Fig. 4(a). The device without graphene exhibits an extinction ratio (ER) of 6∼8 dB. If the graphene is placed onto the top arm waveguide of the device, the ER increases to 10∼12 dB, which is caused by the optical loss of

TABLE I
COMPARISON OF REPORTED ALL-OPTICAL SWITCHES WITH DIELECTRIC MATERIALS

Material	Structure	ER(dB)	Switching time	Integration	FSR	Tuning efficiency (π/mW)
Fiber-Graphene (5 layers) [2]	MZI	20	3.2ms	No	~0.1	0.091
Fiber-Graphene (20 layers) [3]	MZI	19	30ms	No	~0.42	0.188
Fiber-Graphene (5 layers) [34]	Micro ring	13	0.2947ms	No	~1.24	0.114
Fiber-phosphorene [27]	MZI	17	2.5ms	No	0.296	0.029
Si_3N_4-Graphene (1 layer) [23]	Micro ring	10	253ns	Yes	5.4	0.00258
Si_3N_4-Graphene (1 layer) (This work)	MZI	11	571ns	Yes	8.4	0.00917

the arm due to the graphene absorption. In addition, the total loss of the device after graphene transfer is $\sim$4 dB while it is $\sim$ 1 dB for the device without graphene. Thus, the total loss of the device is increased by $\sim$3.1 dB after transferring the graphene, which is also induced by the absorption of graphene.

The switching power and tuning efficiency of the device is then characterized by the CW tuning experiment. Fig. 4(b) depicts the normalized transmission spectra of device measured at different coupled pump powers in the input waveguide. Along with the increase of the pump power, the position of interference fringe has a red shift. When the pump power increases to 109.6 mW, the position of interference fringe shifts $\sim$4.2 nm (a half FSR), leading to a phase shift of π radian for the probe light. Then, a tuning efficiency of 0.0385 nm/mW or 0.00917 π/mW is obtained. Note that, the position of interference fringe for the device without graphene shifts $<$0.2 nm with such a pump power. Thus, one can find that the tuning efficiency is greatly enhanced by graphene absorption. Meanwhile, the tuning efficiency of 0.00917π/mW is much higher than that of the previously reported graphene-on-Si_3N_4 MRR device with a tuning efficiency of 0.00258 π/mW [23]. Moreover, the measured tuning efficiency of 0.00917 nm/mW is a little lower than the aforementioned theoretical tuning efficiency of $\sim$0.012 nm/mW. Such difference might be attributed to the change of the coupling condition between the fiber and waveguide or the propagation loss in the input Si_3N_4 waveguide. Furthermore, one can find that the ER increases when a pump power of 109.6 mW is applied. This might be attributed to the increased Fermi level of graphene from such high pump power. Note that, if the Fermi level increases, the interband absorption of graphene can be suppressed. Then, the graphene-induced loss for the probe light decreases [32] and the ER of the probe transmission spectrum thus increases.

Fig. 4(c) shows the corresponding phase shift of the device under the different injected pump powers, which is deduced from the interference fringe shift. We should find that the phase shift is approximately considered as a linear function of the pump power. Fig. 4(d) presents the tuning efficiency when different pump wavelengths are set. One can note that the tuning efficiency remains unchanged around 0.00917 π/mW since the power coupling ratio of the DCs is insensitive to the wavelength of the injected light. This stands in contrast to the MRR structure, in which the all-optical switching can be implemented only if the pump light wavelength is set at the resonance wavelength.

B. Switching Response Time

Dynamic all-optical switching is then carried out to evaluate the device performance. In this experiment, the pump pulse has a pulse width of 5 μs, a repetition rate of 50 kHz and a duty cycle of 20%. As shown in Fig. 5(a), we set two bias points of the probe light for testing different output probe signal waveforms. When we set the probe wavelength at point A (1514.4 nm), the probe light experienced the transition from "off" state (low transmission) to "on" state (high transmission) periodically along with the variation of the pump power, which is illustrated in Fig. 5 (b). Then we fit the rising and falling edges of the waveform with exponential decay functions $1-\exp(-t/\tau_r)$ and $\exp(-t/\tau_f)$, respectively. The rise and fall time constants of the switch are estimated to be $\tau_r = 571$ ns and $\tau_f = 1.29$ μs, respectively. Here, the rising edge is induced by the heating process and the falling edge is determine by the cooling process. When we set the probe wavelength at point B (1519.9 nm), as shown in Fig. 5(c), the probe also experienced the falling process (heating process) and rising process (cooling process) periodically. After fitting the falling and rising edges of the waveform similarly, the constants of fall and rise time are $\tau_f = 669$ ns and $\tau_r = 1.04$ μs. Note that, our measured switching speed is much faster than that of other MZI thermo-optic switches based on metal heaters [10], [33], which can be attributed to the high thermal conductivity of graphene.

C. Discussion

To further show the performance of our proposed MZI all-optical switch, a comparison between our proposed device and other reported all-optical switches based on dielectric materials

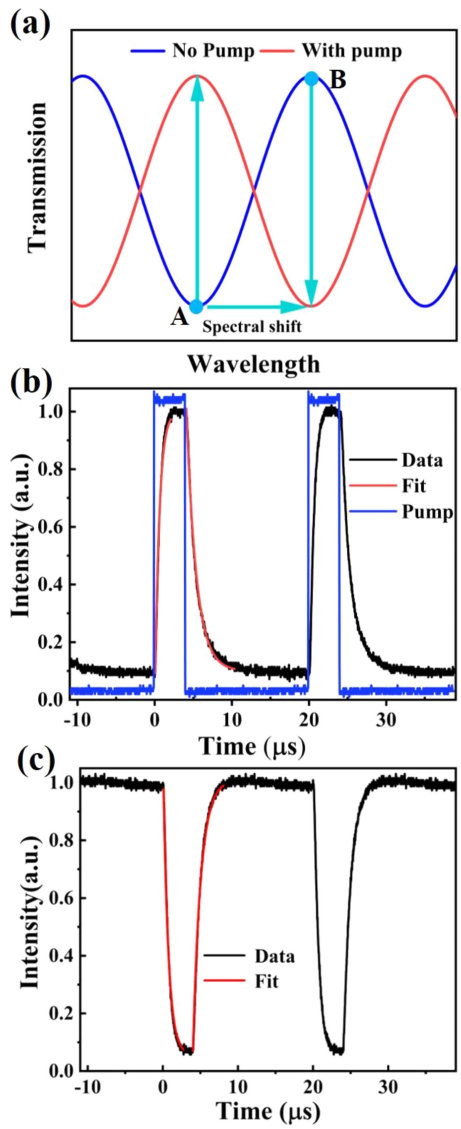

Fig. 5. (a) Illustration of the bias points of the probe light. (b) Waveforms of the pump pulse and probe light biased at point A. (c) Waveform of the probe light biased at point B.

is provided in Table I. One can find that the switching time of our device (∼ns) is much faster than to those (ms) of all-optical switches using fiber-graphene or fiber- phosphorene material [2], [3], [27], [34]. Moreover, our device could achieve a high tuning efficiency which is ∼3.6 times as high as that of the graphene-on-Si_3N_4 MRR all-optical switch [23]. To further improve the tuning efficiency, one could increase the graphene induced absorption by using multi-layer graphene [3] or enlarging the length of graphene. Furthermore, compared to those fiber-based and the MRR based all-optical switches, the FSR of our device is much larger since our integrated device can easily adjust the length difference between the two arms in the MZI structure. Thus, our design can potentially achieve broadband on the insulator platform.

Moreover, based on the experimental data, we also estimate a ±5% variation in the splitting ratio for both DC1 and DC2. Thus, the power splitting ratio of DC1 can vary from 74/26 to 84/16 while the power splitting ratio of DC2 can vary from 45/55 to 55/45. Based on the theoritical analysis, such variations would change the tuning efficiency a little while a high extinction ratio switching can still be expected.

V. Conclusion

In summary, we have proposed and experimentally demonstrated a high-performance MZI all-optical switch based on a graphene-on-Si_3N_4 hybrid structure. Owing to the ultra-high thermal conductivity, graphene could compensate the shortcoming of weak thermo-optic effect of Si_3N_4 material while the insulator nature of Si_3N_4 could eliminate TPA and FCA effects. In the experiment, the device exhibits an extinction ratio of 11 dB and a tuning efficiency of 0.00917 π/mW. Furthermore, the tuning efficiency is insensitive to the wavelength of the pump light. In the dynamic all-optical switching, a rise time constant of $\tau_r = 571$ ns and a fall time constant of $\tau_f = 1.29$ μs are obtained. Based on the experimental results, our proposed configuration could provide a functional integrated component for the development of efficient all-optical control devices with a fast switching speed on the insulator platform.

Acknowledgment

The authors would like to thank the support of device fabrication by the Center for Advanced Electronic Materials and Devices of Shanghai Jiao Tong University.

References

[1] Z. P. Shao, C. Wang, K. Wu, H. Zhang, and J. P. Chen, "Fiber all-optical light control with low-dimensional materials (LDMs): Thermo-optic effect and saturable absorption," *Nanoscale Adv*, vol. 1, no. 11, pp. 4190–4206, Nov. 2019.

[2] X. T. Gan *et al.*, "Graphene-assisted all-fiber phase shifter and switching," *Optica,* vol. 2, no. 5, pp. 468–471, May 2015.

[3] T. Hao, Z. S. Chang, and K. S. Chiang, "Externally pumped low-loss graphene-based fiber Mach–Zehnder all-optical switches with mW switching powers," *Opt. Express,* vol. 27, no. 4, pp. 4216–4225, Feb. 2019.

[4] K. Nozaki *et al.*, "Sub-femtojoule all-optical switching using a photonic-crystal nanocavity," *Nat. Photon.,* vol. 4, no. 7, pp. 477–483, Jul. 2010.

[5] G. Roelkens *et al.*, "III-V/silicon photonics for on-chip and inter-chip optical interconnects," *Laser Photon. Rev.,* vol. 4, no. 6, pp. 751–779, Nov. 2010.

[6] V. R. Almeida, C. A. Barrios, R. R. Panepucci, and M. Lipson, "All-optical control of light on a silicon chip," *Nature,* vol. 431, no. 7012, pp. 1081–1084, Oct. 2004.

[7] G. T. Reed and A. P. Knights, *Silicon Photonics: An Introduction*. London, U.K.: John Wiley & Sons, 2004.

[8] J. S. Levy, A. Gondarenko, M. A. Foster, A. C. Turner-Foster, A. L. Gaeta, and M. Lipson, "CMOS-compatible multiple-wavelength oscillator for on-chip optical interconnects," *Nat. Photon.,* vol. 4, no. 1, pp. 37–40, Jan. 2010.

[9] S. V. Deshpande, E. Gulari, S. W. Brown, and S. C. Rand, "Opticali properties of silicon nltride films deposited by hot filament chemical vapor deposition," *J. Appl. Phys.,* vol. 77, no. 12, pp. 6534–6541, Mar. 1995.

[10] J. Joo, J. Park, and G. Kim, "Cost-Effective 2 x 2 silicon nitride Mach–Zehnder interferometric (MZI) thermo-optic switch," *IEEE Photon. Technol. Lett.,* vol. 30, no. 8, pp. 740–743, Apr. 2018.

[11] S. Romero-Garcia, F. Merget, F. Zhong, H. Finkelstein, and J. Witzens, "Silicon nitride CMOS-compatible platform for integrated photonics applications at visible wavelengths," *Opt. Express,* vol. 21, no. 12, pp. 14036–14046, Jun. 2013.

[12] K. Hirao, K. Watari, M. E. Brito, M. Toriyama, and S. Kanzaki, "High thermal conductivity in silicon nitride with anisotropie microstructure," *J. Amer. Ceram. Soc.,* vol. 79, no. 9, pp. 2485–2488, Jul. 1996.

[13] A. Arbabi and L. L. Goddard, "Measurements of the refractive indices and thermo-optic coefficients of Si_3N_4 and SiO_x using microring resonances," *Opt. Lett.,* vol. 38, no. 19, pp. 3878–3881, Oct. 2013.
[14] G. Cocorullo and I. Rendina, "Thermo-optical modulation at 1.5 μm in silicon etalon," *Electron. Lett.,* vol. 28, no. 1, pp. 83–85, 1992.
[15] F. Wang *et al.*, "Gate-variable optical transitions in graphene," *Science,* vol. 320, no. 5873, pp. 206–209, Apr. 2008.
[16] P. Avouris, "Graphene: Electronic and photonic properties and devices," *Nano Lett,* vol. 10, no. 11, pp. 4285–4294, Nov. 2010.
[17] Q. L. Bao and K. P. Loh, "Graphene photonics, plasmonics, and broadband optoelectronic devices," *ACS Nano,* vol. 6, no. 5, pp. 3677–3694, May. 2012.
[18] S. Q. Yan *et al.*, "Slow-light-enhanced energy efficiency for graphene microheaters on silicon photonic crystal waveguides," *Nat. Commun.,* vol. 8, Feb. 2017, Art. no. 14411.
[19] A. A. Balandin *et al.*, "Superior thermal conductivity of single-layer graphene," *Nano Lett,* vol. 8, no. 3, pp. 902–907, Mar. 2008.
[20] Y. Gao, W. Zhou, X. K. Sun, H. K. Tsang, and C. Shu, "Cavity-enhanced thermo-optic bistability and hysteresis in a graphene-on-Si_3N_4 ring resonator," *Opt. Lett.,* vol. 42, no. 10, pp. 1950–1953, May 2017.
[21] Y. Gao, G. D. Zhou, N. Zhao, H. K. Tsang, and C. Shu, "High-performance chemical vapor deposited graphene-on-silicon nitride waveguide photodetectors," *Opt. Lett.,* vol. 43, no. 6, pp. 1399–1402, Mar. 2018.
[22] J. Q. Wang, Z. Z. Cheng, C. Shu, and H. K. Tsang, "Optical absorption in Graphene-on-Silicon nitride microring resonators," *IEEE Photon. Technol. Lett.,* vol. 27, no. 16, pp. 1765–1767, Aug. 2015.
[23] C. Y. Qiu, Y. X. Yang, C. Li, Y. F. Wang, K. Wu, and J. P. Chen, "All-optical control of light on a graphene-on-silicon nitride chip using thermo-optic effect," *Sci Rep-U.K.,* vol. 7, Dec. 2017, Art. no. 17046.
[24] S. Dwivedi, P. De Heyn, P. Absil, J. Van Campenhout, and W. Bogaerts, "Coarse wavelength division multiplexer on silicon-on-insulator for 100 gbE," in *Proc. IEEE 12th Int. Conf. Group IV Photon.*, 2015, pp. 9–10.
[25] T. Fjelde *et al.*, "Demonstration of 20Gbit/s all-optical logic XOR in integrated SOA-based interferometric wavelength converter," *Electron. Lett.,* vol. 36, no. 22, pp. 1863–1864, Oct. 2000.
[26] Q. F. Xu and M. Lipson, "All-optical logic based on silicon micro-ring resonators," *Opt. Express,* vol. 15, no. 3, pp. 924–929, Feb. 2007.
[27] Y. Z. Wang *et al.*, "All-Optical phosphorene phase modulator with enhanced stability under ambient conditions," *Laser Photon. Rev.,* vol. 12, no. 6, pp. 1–9, Jun. 2018.
[28] A. E. Willner, S. Khaleghi, M. R. Chitgarha, and O. F. Yilmaz, "All-Optical signal processing," *J. Lightw. Technol.,* vol. 32, no. 4, pp. 660–680, Feb. 2014.
[29] L. H. Yu, Y. L. Yin, Y. C. Shi, D. X. Dai, and S. L. He, "Thermally tunable silicon photonic microdisk resonator with transparent graphene nanoheaters," *Optica,* vol. 3, no. 2, pp. 159–166, Feb. 2016.
[30] Z. Z. Xu *et al.*, "Ultra-compact tunable silicon nanobeam cavity with an energy-efficient graphene micro-heater," *Opt. Express,* vol. 25, no. 16, pp. 19479–19486, Aug. 2017.
[31] Y. Gao, L. Tao, H. K. Tsang, and C. Shu, "Graphene-on-silicon nitride waveguide photodetector with interdigital contacts," *Appl. Phys. Lett.,* vol. 112, no. 21, pp. 1–5 May 2018.
[32] C. Y. Qiu, T. Pan, W. L. Gao, R. L. Liu, Y. K. Su, and R. Soref, "Proposed high-speed micron-scale spatial light valve based on a silicon-graphene hybrid structure," *Opt. Lett.,* vol. 40, no. 19, pp. 4480–4483, Oct. 2015.
[33] P. Dong *et al.*, "Low power and compact reconfigurable multiplexing devices based on silicon microring resonators," *Opt. Express,* vol. 18, no. 10, pp. 9852–9858, May 2010.
[34] Y. D. Wang *et al.*, "All-optical control of microfiber resonator by graphene's photothermal effect," *Appl. Phys. Lett.*, vol. 108, no. 17, pp. 1–5, Apr. 2016.